ACS APPLIED MATERIALS & INTERFACES

Research Article

www.acsami.org

Transparent Conductive Oxide Films Embedded with Plasmonic Nanostructure for Light-Emitting Diode Applications

Shih-Hao Chuang,[†] Cheng-Sheng Tsung,[†] Ching-Ho Chen,[†] Sin-Liang Ou,[†] Ray-Hua Horng,[§,⊥] Cheng-Yi Lin,[§] and Dong-Sing Wuu*[,†,‡]

[†]Department of Materials Science and Engineering, National Chung Hsing University, Taichung 40227, Taiwan

[‡]Department of Materials Science and Engineering, Da-Yeh University, Changhua 51591, Taiwan

[§]Institute of Precision Engineering, National Chung Hsing University, Taichung 40227, Taiwan

[⊥]Advanced Optoelectronic Technology Center, National Cheng Kung University, Tainan 70101, Taiwan

ABSTRACT: In this study, a spin coating process in which the grating structure comprises an Ag nanoparticle layer coated on a *p*-GaN top layer of InGaN/GaN light-emitting diode (LED) was developed. Various sizes of plasmonic nanoparticles embedded in a transparent conductive layer were clearly observed after the deposition of indium tin oxide (ITO). The plasmonic nanostructure enhanced the light extraction efficiency of blue LED. Output power was 1.8 times the magnitude of that of conventional LEDs operating at 350 mA, but retained nearly the same current−voltage characteristic. Unlike in previous research on surface-plasmon-enhanced LEDs, the metallic nanoparticles were consistently deposited over the surface area. However, according to microstructural observation, ITO layer mixed with Ag-based nanoparticles was distributed at a distance of approximately 150 nm from the interface of ITO/*p*-GaN. Device performance can be improved substantially by using the three-dimensional distribution of Ag-based nanoparticles in the transparent conductive layer, which scatters the propagating light randomly and is coupled between the localized surface plasmon and incident light internally trapped in the LED structure through total internal reflection.

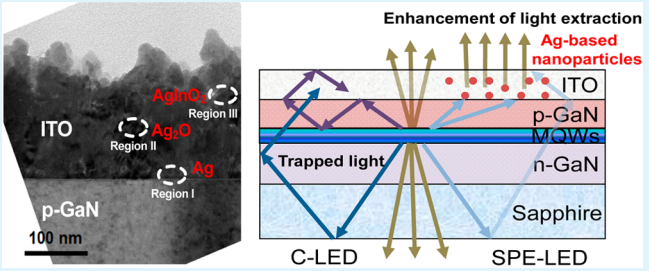

KEYWORDS: *light-emitting diodes, light extraction efficiency, nanoparticles, surface plasmons, transmission electron microscopy*

1. INTRODUCTION

Group III nitride compound semiconductors used to fabricate high-brightness light-emitting diodes (LEDs) at wavelengths from the ultraviolet to visible region have attracted much attention.[1−4] Although LEDs are commercially available, they are flawed by inefficiency caused by low internal quantum efficiency (IQE) and poor light extraction efficiency (LEE) from semiconductor light sources. IQE is strongly influenced by the nonradiative recombination process of threading dislocations and other defects, and by the separation of the electron and hole wave functions caused by spontaneous polarization and strain-induced piezoelectric polarization.[5,6] Another source of energy loss is total internal reflection (TIR), which occurs at the emitter/air (or epoxy) interface because of the typically high refractive index of the emitting materials.[7,8] Therefore, the most critical requirement for a high-power solid-state LED is developing new methods to increase the IQE or LEE of the devices.

Surface plasmons (SPs) excited by the interaction between light and metal surfaces can enhance light absorption in molecules[9−11] and increase Raman scattering intensities.[12−14] Fluctuations in electromagnetic fields, called surface plasmon polaritons (SPPs), accompany the charge fluctuation of the SP oscillation. However, when the resonant frequency of the SPPs overlaps the emission frequency of the quantum wells (QWs) at the metal and semiconductor interface, the QW energy can transfer to the SPs, in which case, electron−hole recombination can produce SPPs instead of photons or phonons. Because the density of SPP mode states is large, the QW−SP coupling rate should be rapid, and the new path of a recombination increases the spontaneous emission rate of the device.[15−17] If the metal/semiconductor surface were perfectly flat, extracting light from the SPP mode would be difficult and the SP energy would thermally dissipate. SPP energy can be extracted as light by using rough metal film, which allows high-momentum SPPs to scatter, lose momentum, and couple, forming radiative light.[18] However, only a few LEDs can be enhanced using SPP−emitter coupling because the SPP resonant frequency of a metal film is difficult to tune.[19,20] Unlike SPPs on a metal film, the local collective oscillations of electrons at interfaces between metallic nanoparticles and dielectric matrices are localized surface plasmons (LSPs). Generally, metallic nanoparticles are formed through the thermal annealing of a thin metal layer. By controlling the thickness of the deposited metal layer and the

Received: October 28, 2014
Accepted: January 6, 2015
Published: January 6, 2015

DOI: 10.1021/am507481n
ACS Appl. Mater. Interfaces 2015, 7, 2546−2553

annealing conditions, metallic nanoparticles of various sizes, shapes, and periodic distances can be tuned to induce LSPs possessing various resonance energies. In addition, the LSPs improved LED performance over SPPs ones result from less dissipation because the induced electromagnetic wave is locally confined and cannot propagate along the metal surface. The metal layer is no longer opaque, enabling emission from the metal side.

In previous studies investigating SP-enhanced GaN-based LEDs, a metallic nanoparticle layer was embedded in the *p*-GaN layer.[21−25] The coupling of spontaneous emission from InGaN/GaN multiple quantum wells (MQWs) with the LSP modes of metal/dielectric nanostructures can enhance light emission by improving the IQE of the device. However, the penetration depth of the SP evanescent field, estimated to be merely tens of nanometers for a blue emitting wavelength, depends on the distance between the QWs and the metallic structures.[26−28] Nevertheless, the *p*-GaN layer in blue emissive GaN-based LEDs, sandwiched between the active and *p*-type conducting layers, must exceed a 100 nm thickness to ensure sufficient carrier mobility. Therefore, the crystal quality and electrical characteristics of such SP-enhanced LEDs are degraded because the *p*-GaN is too thin to facilitate formation of a *p*−*n* junction, and the metallic nanoparticles embedded in the GaN layer induce defects.[23]

Although the IQE enhancement via QW−LSP coupling of LEDs has been studied, only a few cases in which the LEE is enhanced by LSP−TM light coupling have been reported. In some situations, because the distance between the metallic nanoparticles and MQWs is long, enhancement through emitter−field interaction is no longer applicable. Thus, the energy of the generated photons in the active layers is first transferred to the metallic nanoparticles, inducing LSPs and then light emission. For LED structures grown on a *c*-plane substrate, the transverse-electric TE (or transverse-magnetic TM) polarization direction corresponds to the electric field perpendicular (or parallel) to the *c*-axis. Because TE-light propagates mainly in the vertical direction, it can easily escape from the LED chip through the substrate direction. However, the TM-light propagates mainly in the lateral direction, severely affected by TIR because of the large incident angle on the interface, and emission light only escapes from the top and bottom surfaces when inside an escape cone. Because of the various propagation directions, the LEE of the TE mode is higher than that of the TM mode in most LED structures.[29] Moreover, a ratio of approximately 1.8:1 has been observed between electroluminescence (EL) intensities with polarized TE and TM modes in blue LEDs,[30] suggesting that blue photons cannot be entirely extracted from the escape cone. An LSP−TM light resonance condition enables the metallic nanoparticles to capture the trapped TM-light in the epitaxial layers of LED devices and enhances the LEE,[31−33] an improvement that only results from an out-coupling of the generated photons by the metallic nanoparticles. Although the IQE of LEDs is not enhanced by QW−LSP coupling, the LEE of this device is enhanced by the LSP−TM light coupling.

In this study, an SP-enhanced LED (SPE-LED) was successfully fabricated by improving the LEE of the device through LSP−TM light coupling instead of QW−LSP coupling. The distance between the Ag nanoparticles and InGaN/GaN MQWs is too thick to allow the QW−LSP coupling. A spin coating process, which used a grating structure composed of a nano-Ag solution coated on a *p*-GaN layer, facilitated rapid processing time, high production yield, lower cost, and high uniformity on the curved surface. Moreover, the size, density, and periodic distance of metallic nanostructures were controlled by adjusting the spin coating rate, heat treatment condition, and nano-Ag solution concentration. An electron beam was used to evaporate 200 nm-thick indium tin oxide (ITO) for use as an ohmic contact layer, which was deposited on the Ag nanoparticle top layer. During the physical vapor deposition, the Ag nanoparticles were embedded in the ITO layer, forming the Ag-based plasmonic nanostructure. The structural properties of ITO/*p*-GaN with Ag nanoparticles were investigated through atomic force microscopy (AFM), field-emission scanning electron microscopy (FESEM), and transmission electron microscopy (TEM). LED performance was substantially improved by the three-dimensional distribution of Ag-based nanoparticles. To validate the superior performance of SPE-LEDs, conventional LEDs (C-LED) without Ag nanoparticles were also fabricated for comparison.

2. EXPERIMENTAL SECTION

The blue LED wafers used as the samples in this experiment consisted of a typical GaN-based LED structure grown on a c-plane (0001) sapphire through metal−organic chemical vapor deposition (MOCVD). The epilayers of the LED structure, listed in order from substrate to surface, were as follows: a 0.03 μm thick GaN nucleation layer; a 2.7 μm thick GaN undoped layer; a 3.0 μm thick *n*-GaN layer; 10 pairs of InGaN/GaN MQWs; 0.025 μm thick Mg doped *p*-AlGaN; and 0.2 μm thick *p*-GaN. To coat the Ag nanoparticles on the *p*-GaN top layer, the samples were removed from the MOCVD chamber. Spin coating using a nano-Ag solution (in which the average Ag-particle diameter was approximately 20 nm) was employed, and after the nano-Ag solution was uniformly coated on the *p*-GaN layer, the Ag layer was transformed to Ag nanoparticles during baking at 130 °C for 1 min. The metallic nanoparticle layer was then fabricated, and a baking process enabled the metallic nanoparticles to self-aggregate. Because the optical response of the metallic nanoparticles depended on the size, shape, and density, controlling the nanostructure by modulating the concentration of the nano-Ag solution with the proper spin coating rate was beneficial. In addition, a 200 nm thick ITO film, the transparent conductive layer, was deposited on the Ag nanoparticle layer through electron-beam evaporation, and subsequently thermally annealed at 550 °C for 5 min in an ambient atmosphere. To fabricate the LEDs, the mesa was partially etched using an inductively coupled plasma etching process featuring Cl_2 source gases until the *n*-GaN layer was exposed for *n*-type ohmic contact. Finally, the Ti, Al, Ti, Cr, and Au layers (15 nm, 2000, 15, 5, and 200 nm, respectively) were deposited onto samples to form *n*-pad and *p*-pad electrodes. The blue SPE-LED was 1 × 1 mm. For comparison, the *p*-GaN layer of a conventional LED without Ag nanoparticles was also fabricated.

3. RESULTS AND DISCUSSION

After the nano-Ag solution was uniformly coated on the *p*-GaN top layer in a spin coating process, a Ag layer was formed, and subsequently transformed into Ag nanoparticles during baking at 130 °C for 1 min. Figure 1 depicts AFM images of the Ag nanoparticles created using nano-Ag solutions with concentrations of 100 and 10 ppm, respectively, on the *p*-GaN top layers. Because of the high uniformity on the surface of curved parts during a spin coating process, the root-mean-square (RMS) roughnesses for the two samples were 1.18 and 3.90 nm, respectively. Compared with the as-grown *p*-GaN epilayer (RMS = 0.95 nm), the grating structure on the *p*-GaN top layer that had a low surface roughness was naturally formed through the self-aggregation of Ag nanoparticles. However, Ag nanoparticle size increased and their shapes became more irregular

DOI: 10.1021/am507481n
ACS Appl. Mater. Interfaces 2015, 7, 2546−2553

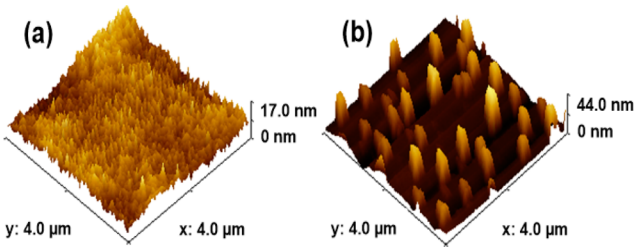

Figure 1. AFM images of the surface with (a) 100 ppm and (b) 10 ppm concentrations of the nano-Ag solutions coated on *p*-GaN top layer after a baking process, respectively.

as the concentration of nano-Ag solution increased; the size and shape of the Ag nanoparticles determined the resonance energy of the generated LSP.

Figure 2 illustrates the conductive atomic force microscopy (C-AFM) images, including the surface morphology and

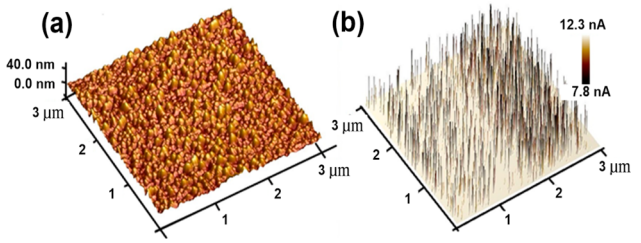

Figure 2. (a) Topographic image of ITO thin film embedded with Ag-based nanoparticles. (b) Current distribution image of ITO layer embedded with Ag-based nanoparticles at a sample bias voltage of 500 mV.

current distribution of an as-deposited ITO thin film on the Ag nanoparticle layer (the sample fabricated using a nano-Ag solution with 10 ppm concentration). C-AFM is a powerful current-sensing technique that enables studying insulating materials on the nanometer scale. Figure 2a illustrates the surface morphology, in which ITO grains have maximal diameters of approximately 100 nm and protrude from the film plane by a few tens of nanometers. The current distribution image for bias voltages at the tip of 500 mV was measured in the same sample area depicted in the surface morphology image. In the current distribution image shown in Figure 2b, much of the scanned areas exhibited a current higher than the 12 nA sensitivity of the amplifier (white areas), because the ITO thin film was a transparent conductive layer with low resistance. However, the image reveals isolated regions of current signals that have an average diameter of approximately 20 nm. These regions exhibit a local minimum of the measured current (black areas), and are hereafter called "spots." This article focuses on the characterization of these spots.

To confirm the existence of Ag-based nanoparticles embedded in a transparent conductive layer on the *p*-GaN, the LED epitaxial structure with an ITO layer was soaked in a hot HCl solution (the sample also fabricated using the nano-Ag solution with a 10 ppm concentration). After a 1.5 min wet etching process, a portion of the ITO top layer was etched out (etching depth ~ 100 nm), and the Ag-based nanoparticles below the surface were exposed. Figure 3a depicts FESEM micrographs, which clearly show the various sizes of Ag-based nanoparticles embedded in the ITO layer after the deposition

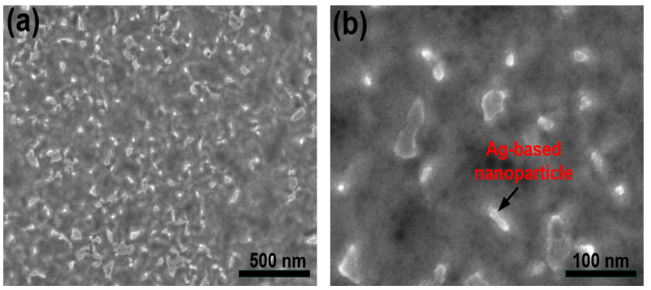

Figure 3. (a) Plane-view FESEM micrographs of the ITO film embedded with Ag-based nanoparticles (the sample fabricated by nano-Ag solution with 10 ppm concentration) after the wet etching process. An enlarged FESEM image is shown in panel b.

of the ITO film (~200 nm). The acid resistance of the transparent conductive layer increased because of the existence of the Ag-based nanoparticles. The high-FESEM-magnification image shown in Figure 3b indicates that the diameter and density of Ag-based nanoparticles were between 20 and 80 nm and 8.47×10^9 cm^{-2}, respectively, and each ITO layer covered approximately 15.67% of the surface area. Based on these results, most Ag-nanoparticles presented in this study were embedded in the ITO film.

In addition to FESEM imaging, the ITO film embedded with Ag-based nanoparticles that had grown on the *p*-GaN layer was also analyzed through TEM plane-view observation. To prepare a sample for TEM measurement, the substrate, LED epilayers, and a portion of the ITO film were ground. An approximately 80 nm thick ITO film remained on the thin region of the TEM sample. Figure 4 depicts the TEM bright field image and the

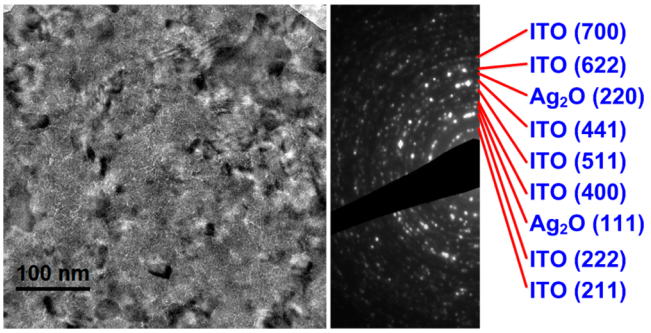

Figure 4. TEM bright field image and corresponding electron diffraction pattern of the ITO film embedded with Ag-based nanoparticles (the sample fabricated by nano-Ag solution with 10 ppm concentration).

corresponding electron diffraction pattern of the sample. Several nanoparticles with an average size of 35 ± 10 nm were distributed randomly in the ITO film. The feature of TEM image was similar to that of FESEM image. The electron diffraction pattern was analyzed to determine the crystal structure of the sample, and many diffraction rings were observed, indicating that the structure of the sample was polycrystalline. As expected, the majority of the diffraction rings were indexed to the ITO crystalline phase. In addition, two diffraction rings belonging to the $Ag_2O(111)$ and $Ag_2O(220)$ planes were formed in the pattern. Therefore, the Ag_2O phase could be attributed to the Ag-based nanoparticles formed in the ITO film.

DOI: 10.1021/am507481n
ACS Appl. Mater. Interfaces 2015, 7, 2546−2553

To determine the transition and distribution of Ag nanoparticles after the ITO layer evaporated, the LED samples were subjected to high-resolution TEM (HR-TEM) measurement. Coated Ag nanoparticles formed using nano-Ag solutions with concentrations of 10 and 100 ppm embedded in the ITO layers. Figure 5 depicts TEM images of the nano-Ag solution

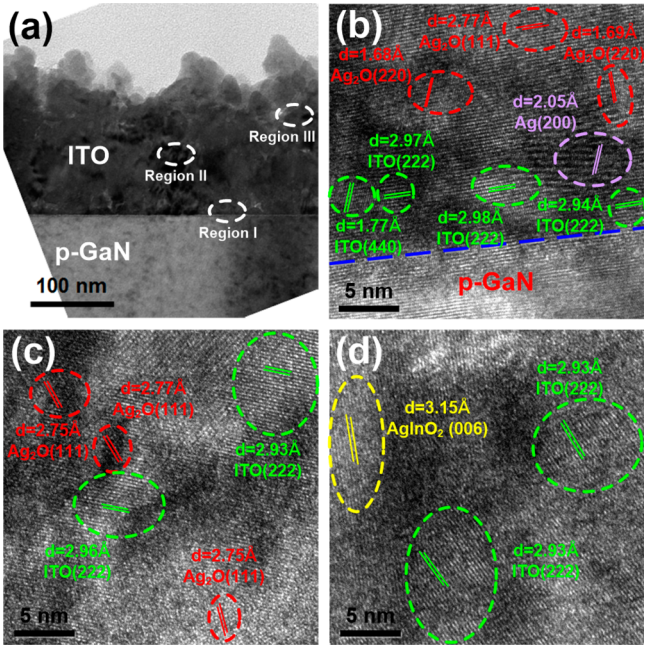

Figure 5. (a) Cross-sectional TEM images of ITO film embedded with Ag-based nanoparticles on the *p*-GaN top layer (using the nano-Ag solution with 10 ppm concentration). HR-TEM images for this sample were focused on (b) region I, (c) region II and (d) region III, as marked in Figure 5a.

with the 10 ppm concentration. In the cross-sectional TEM image (Figure 5a), which was used to examine the ITO grown on the *p*-GaN layer, the interface of ITO/*p*-GaN was clearly apparent, and the ITO layer was approximately 200 nm thick. Three regions (marked I, II, and III in Figure 5a), comprising the interface between *p*-GaN and ITO, and the middle and upper parts of the ITO layer, were selected in which to perform HR-TEM measurement (Figure 5b–d). As shown in the HR-TEM image of the ITO/*p*-GaN interface (Figure 5b), numerous ITO grains aggregated on the *p*-GaN layer, and nearly no Ag grain was present. When imaging was captured at a distance of approximately 10 nm from the interface to ITO, a Ag grain approximately 10 to 20 nm was observed; when the distance was greater than 15 nm, several grains in the Ag_2O phase were visible, indicating that the Ag nanoparticles coated on the *p*-GaN layer and suspended to form the ITO layer evaporated. Additionally, Ag nanoparticles reacted with oxygen atoms to form the Ag_2O phase. When the nanosized Ag particles (≤20 nm) acquired sufficient energy and melted, the Ag particles reacted with gaseous atoms, forming the Ag_2O phase that was embedded in the ITO layer. The Ag_2O phase was also observed in the middle of the ITO layer (Region II). Figure 5c shows Ag_2O grains approximately 25 ± 10 nm in size. In the upper part of the ITO layer (Figure 5d), the Ag and Ag_2O grains disappeared. Based on the analysis depicted in Figure 5d, *d*-spacing evaluated to 2.93 Å was indexed to the ITO (222) plane. In addition to the ITO grains, other *d*-spacings greater than 3.15 Å had formed (Figure 5d), belonging to the 3R-polytype $AgInO_2$(006) plane.[34] The $AgInO_2$ formation indicated that the Ag nanoparticles contributed to the ITO evaporation process and created the other solid phase.

A nano-Ag solution with a concentration of 100 ppm was used to embed Ag into the ITO layer, and a similar TEM measurement was applied (Figure 6). Figure 6a shows a cross-

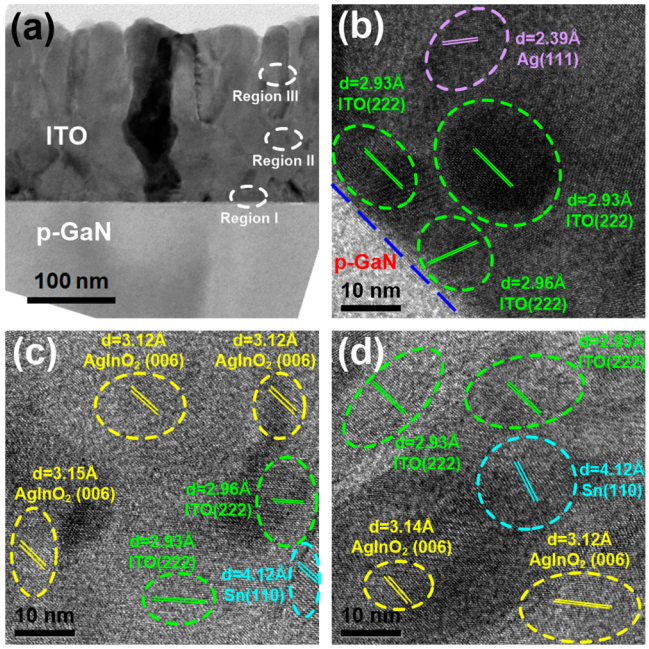

Figure 6. (a) Cross-sectional TEM images of ITO film embedded with Ag-based nanoparticles on the *p*-GaN top layer (using the nano-Ag solution with 100 ppm concentration). HR-TEM images for this sample were focused on (b) region I, (c) region II, and (d) region III, as marked in panel a.

sectional TEM image focused on the ITO/*p*-GaN region. After the Ag nanoparticles were coated on the *p*-GaN layer, a 200 nm thick ITO layer was evaporated. Regions I, II and III marked in Figure 6a were subjected to HR-TEM measurements, depicted in Figure 6b–d, respectively. The interfaces between *p*-GaN and ITO, and the middle and upper parts of the ITO layer were also indicated in the regions, respectively. As shown in Figure 6b, the ITO grains formed on the *p*-GaN layer, and the Ag nanoparticle was approximately 30 nm from the *p*-GaN layer, suggesting the Ag nanoparticle was suspended in this sample. HR-TEM measurements on the middle and upper parts of ITO layer (Figure 6c, d) indicated that the two regions had similar microstructures. In addition to the ITO phase formed with *d*-spacings of 2.93 to 2.96 Å, various *d*-spacings, ranging from 3.12 to 3.15 Å indexed to the $AgInO_2$ phase, were apparent in these two regions, suggesting that the Ag nanoparticles in this sample were embedded in the ITO layer with a distance of approximately 150 nm (Figure 6a) and reacted with oxygen and indium atoms. Nearly no Ag_2O phase was present in the sample. By contrast, a large *d*-spacing of 4.12 Å was indexed to the Sn(110) plane (Figure 6c,d); the Sn phase was observed only in the image shown in Figure 6. When the Ag concentration of nano-Ag solution was increased to 100 ppm, increasingly more Ag atoms reacted with the oxygen and indium atoms, creating the $AgInO_2$ phase, and the Sn phase resulted from the unreacted Sn atoms. Compared with the

DOI: 10.1021/am507481n
ACS Appl. Mater. Interfaces 2015, 7, 2546–2553

sample using the nano-Ag solutions with 10 ppm concentrations, the amount of $AgInO_2$ phase substantially increased with greater Ag concentration. According to previous research,[35] $AgInO_2$ film exhibits poorer electrical properties with a resistivity of 1.7×10^{-1} Ω·cm, than does conventional ITO film. In this study, when the LED devices were fabricated, the sample embedded with Ag nanoparticles created using the nano-Ag solution with a 10 ppm concentration exhibited improved optoelectronic performance, compared with the C-LED. When the nano-Ag solution with a 100 ppm concentration was used, the electronic performance of the LED deteriorated, which is attributable to the $AgInO_2$ phase that formed in the ITO layer; the electrical property of the ITO worsened, resulting in poor ohmic contact between the ITO film and the *p*-GaN layer.

According to the results shown in Figures 1–6, the mechanism of Ag nanoparticles embedded in ITO film from the ITO/*p*-GaN interface can be evaluated as follows. First, the Ag nanoparticles formed during self-organized agglomeration, after the nano-Ag solution was uniformly coated on the *p*-GaN top layer and baked. During physical vapor deposition, the target material (ITO) was transferred from the solid phase to the vapor phase atom by atom, and then back to the solid phase. Because the Ag nanoparticles (approximately 20 nm) exhibited a lower melting point (approximately 150 °C) than did the Ag bulk (approximately 960 °C). During reactive deposition, the depositing material reacted with the gaseous environment and molten Ag nanoparticles of the codeposited material, forming a grain and gradually building a film on the surface of *p*-GaN. Because the Ag nanoparticles and *p*-GaN layer did not form a chemical bond during the baking process, the various sized Ag-based nanoparticles of the compound material embedded in the ITO layer (Figure 7).

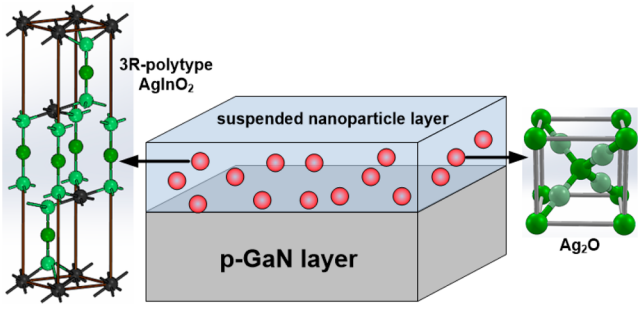

Figure 7. Schematic Ag-based nanoparticles embedded in ITO layer compound for Ag_2O and 3R-polytype $AgInO_2$ along the *c*-axis.

In previous studies that focused on surface-plasmon-enhanced LED devices,[21−25] the metallic nanoparticles were consistently distributed over the *p*-GaN surface area, which indicated that the improved performance of the LEDs was caused by the two-dimensional distribution of nanoparticles through MQW−LSP coupling. However, in this study, the Ag nanoparticles embedded throughout most of the ITO layer. Thus, improved LED performance can be facilitated by the three-dimensional distribution of Ag-based nanoparticles. Figure 8 shows the transmission spectrum of the Ag-based nanoparticles embedded in the ITO layer. The ITO/sapphire samples created using nano-Ag solution concentrations of 10 to 100 ppm exhibited optical curves. As shown in Figure 8a, a primary absorption peak of Ag-based nanoparticle varied from 377 to 385 nm, attributable to the excitation of the dipole

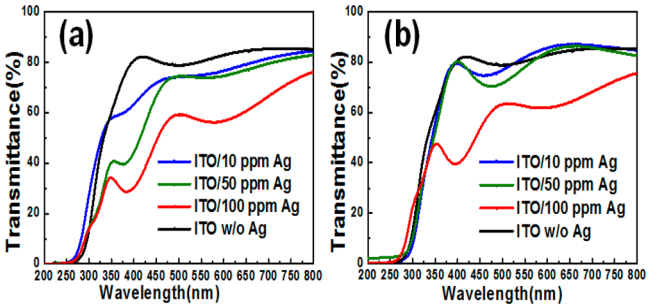

Figure 8. Transmittance spectrum of ITO and ITO embedded Ag-based nanoparticles with various nano-Ag solution concentrations: (a) as-deposited state and (b) annealing at 550 °C in atmosphere.

plasmon mode. The absorption peaks of the samples were located in the near-ultraviolet region, distinct from those only located at the blue wavelength region.[21,22] Because of the varying nanoparticle size and shape in the ITO layer, the LSP modes of various resonance energies created broad transmission dips and increased when the concentration of the nano-Ag solution increased. In general, wavelengths correspond to transmission dip redshifts; the dip broadens as the average size of Ag-based nanoparticles increases; the absorption intensity is determined by the amount of nanoparticles.

Figure 8b shows the transmittance of the ITO samples annealed at 550 °C in an ambient atmosphere. As the diameter of Ag-based nanoparticles increased during the thermal annealing process, the localized SP resonance (LSPR) wavelength lengthened and broadened, and a strong dip appeared near 395 nm in the 100 ppm sample. In samples with higher Ag concentrations (100 ppm), the dip near 395 nm was caused by the SPP resonance generated at the interface of ITO and *p*-GaN, a result that was similar to that obtained from the optical transmission spectra of the Ag/ITO composite films.[36] However, precisely estimating the LSPR wavelength is difficult because of the randomly distributed plasmonic nanostructure in the ITO layer. A range of various wavelength shifts in the LSPR can be expected. The LSPR wavelength belonging to the 10 ppm sample exhibited an absorption peak at 463 nm, which was the lowest observed in this study. Because the prepared LED sample emitted 455 nm of light, the 10 ppm sample could enhance emission efficiency.

Figure 9a depicts the photoluminescence (PL) spectra of InGaN/GaN MQW blue LEDs with and without Ag-based nanoparticles embedded in ITO film. The PL spectra was

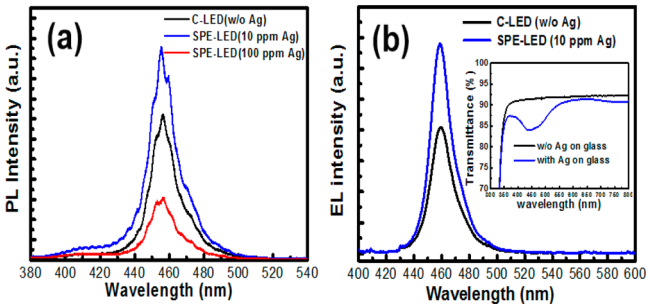

Figure 9. (a) Room temperature PL spectra of the blue LEDs with and without Ag nanoparticles. (b) EL spectra of the LED samples with and without Ag nanoparticles when the injection current is 20 mA. The inset shows the transmission spectra of only Ag nanoparticles on the glass substrate.

DOI: 10.1021/am507481n
ACS Appl. Mater. Interfaces 2015, 7, 2546−2553

obtained by measuring the top side of the samples at room temperature, using a He−Cd laser (λ = 325 nm) that had an excitation laser power of 40 mW. Unlike the C-LED, the ITO film embedded with Ag-based nanoparticles of LED exhibited a PL intensity of enhancement and suppression in the 10 and 100 ppm samples, respectively. In the 10 ppm sample, the integrated PL intensity of the LED increased 52.5%, compared with that of the C-LED. The LSPR wavelength (463 nm) of the Ag-based nanoparticles coincided with the emission wavelength (455 nm) of the LED, enhancing the PL through the LSP−TM light coupling. This enhancement was attributable to the plasmonic nanostructure embedded in the ITO layer, which coupled with the trapped TM light in the ITO/*p*-GaN interface and the ITO layer, and subsequently emitted light. By contrast, PL intensity was suppressed in the 100 ppm sample because the transmittance at 455 nm was lower than 60%. The density of state of these dipole plasmon modes achieved a maximum of approximately 395 nm, indicated by the dip in the 100 ppm curve (Figure 8b). Because of the momentum disparity between the SPP and photon and the high dissipation rate, PL intensity was suppressed. In addition, the coupling on the high-energy side of the PL spectrum in the 100 ppm sample caused a 2 nm blueshift in the spectral center of mass compared with that of C-LEDs.

Figure 9b shows the electroluminescence (EL) spectra of the LED without and with Ag nanoparticles (10 ppm sample) at low injection current (@20 mA). It was found that the EL peaks of these LEDs are located at the blue wavelength region. The inset of Figure 9b shows the transmission spectra of only Ag nanoparticles on the glass substrate using a nano-Ag solution by spin coating process. Compared to spectra of Ag-based nanoparticles embedded in ITO layer (Figure 8a), the spectrum of the Ag nanoparticles exhibits an absorption peak at 437 nm, which resulted from the extinction by the excitation of dipole plasmon modes in the Ag nanoparticle with regard to its size, density, and periodic distance of nanostructures. This is the unique SP band in absorption spectrum of pure Ag nanoparticles, and the LSPR wavelength of pure Ag nanoparticle is matched with the emission wavelength of the light emitted from LED. Therefore, the LSP−light coupling effect on the high-energy side of the EL spectrum in SPE-LED leads to the blueshift by 2 nm of its emission peak wavelength with respect to that of C-LED. The spectral blueshift of SPE-LED also supports the LSP−TM light coupling effect. Moreover, the LSP−TM light coupling results in quite effective emission, leading to 70% enhancement in EL peak intensity compared with that of the C-LED. If the LSPR wavelength is closer to the emission wavelength of LED, more efficient coupling to LSP can be expected. Especially, the transmittance of pure Ag nanoparticles on the glass substrate is higher than 84%, indicating that the improvement of light out is not fully due to the scatterings by the Ag nanoparticle layer. Owing to the results of optical transmission, PL and EL spectra mentioned above, it has the concrete evidence that the improvement in the light out is due to LSP−TM light coupling effect.

To determine the optoelectronic performance of SPE-LEDs, the current−voltage (I−V) characteristics and optical output power were measured. As Figure 10a shows, the SPE-LED forward voltages for the 10 and 100 ppm samples, measured using an injection current of 20 mA, were 3.04 and 8.17 V, respectively. The forward voltage of 20 mA in the C-LED without Ag nanoparticles on the *p*-GaN top layer was 3.03 V, indicating that the lower Ag-concentration samples did not

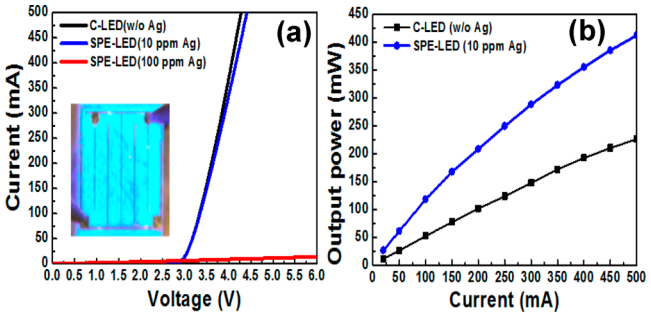

Figure 10. (a) Typical current−voltage characteristics of SPE-LED samples fabricated with different concentration of a nano-Ag solution. (b) Light output power as a function of injection current for SPE-LED and C-LED.

degrade the electrical properties, because a small amount of $AgInO_2$ nanoparticles were formed by the Ag nanoparticles embedded at the ITO/*p*-GaN interface. In the 10 ppm sample, most of the low resistivity Ag_2O was embedded in the ITO layer, evident from the microstructural observation of HR-TEM measurement. In addition, *p*-GaN thickness in the SPE-LEDs was sufficient to facilitate formation of a *p*−*n* junction that improved the electrical property. Only 4.03 V was required to enable the 350 mA current to flow into the 10 ppm device, a result that is an optimal result for surface-plasmon-enhanced blue LEDs with low series resistance.[21−25] The series resistance of the SPE-LEDs in this study gradually increased with the increasing density of the Ag nanoparticles. When the nano-Ag solution with a concentration of 100 ppm was used, the I−V characteristic of the SPE-LEDs degraded because of the nonoptimized ohmic contact property at the ITO layer that was due to the thick $AgInO_2$ film with high resistivity. In addition, the transmittance of the SPE-LED devices in the blue wavelength region was low (Figure 8b). Therefore, in this study, the optical performance of SPE-LEDs embedded with Ag nanoparticles created using the nano-Ag 100 ppm solution was not investigated.

As Figure 10b illustrates, device performance was measured according to the light output power as a function of the injection current. A 88.10% enhancement in output power was achieved when the injection current was 350 mA because the I−V characteristics and LSP resonance effect were excellent. Figure 11 depicts a schematic diagram of the enhanced light-output mechanisms. The three-dimensional distribution of Ag-based nanoparticles in the ITO layer scatters the propagating light randomly, forms an optical microcavity, and couples the localized SP and TM-light internally trapped by the TIR in the ITO/*p*-GaN interface and the ITO layer. The LSP−TM light

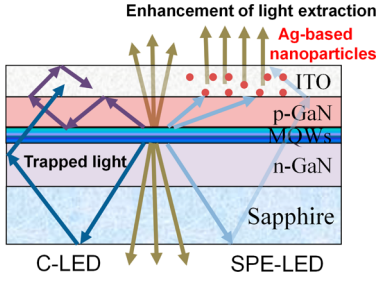

Figure 11. Schematic diagram of light output enhanced mechanisms of SPE-LED in comparison with the C-LED.

DOI: 10.1021/am507481n
ACS Appl. Mater. Interfaces 2015, 7, 2546−2553

coupling suggested that Ag-based nanoparticles coupled with the trapped light in the device, and then radiated to the outside of the device, enhancing the light extraction efficiency of the LEDs.

To confirm this hypothesis, the far-field radiation patterns (at 350 mA) of SPE-LEDs using the 10 ppm sample and of C-LED were measured for a chip that was not encapsulated by epoxy. The normal direction and large-angle far-field pattern of the SPE-LEDs were more enhanced that those of the C-LED (Figure 12). Viewing angles of 153° and 144° were also

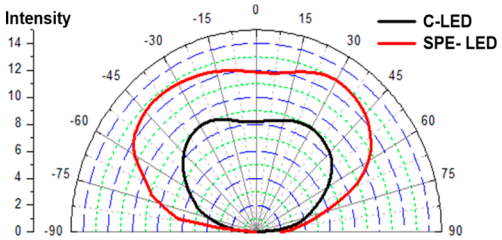

Figure 12. Far-field emission patterns of the SPE-LEDs and C-LEDs at the injection current of 350 mA.

measured for the SPE-LEDs and C-LED, respectively. The overall integrated area of the SPE-LED electroluminescence intensity was larger than that of the C-LED, because the LSP−TM light coupling effect, microcavity effect and multiple scattering caused by the Ag-based nanoparticles embedded in ITO increased the light extracted from the ITO/*p*-GaN interface and the ITO layer to air transition. These results indicated that the three-dimensional distribution of Ag-based nanoparticles embedded in the ITO layer efficiently increased the light extraction at large angular directions and enhanced light diffusion.

4. CONCLUSIONS

In this study, the light output of GaN-based LEDs using a novel transparent conductive oxide film embedded with plasmonic nanostructure on the *p*-GaN top layer was enhanced. Because the Ag-based nanoparticles embedded throughout most of ITO layer, the three-dimensional distribution of metallic nanoparticles in the ITO layer scatters the propagating light randomly, forms an optical microcavity, and couples the LSP and TM-light. Measurement of the PL intensity, EL intensity and large-angle far-field emission pattern of the SPE-LEDs indicated that the light extraction efficiency increased substantially during LSP−TM light coupling. The optoelectronic property of the conventional LED sample suggested the superior performance of the SPE-LEDs (fabricated with lower Ag-concentration samples), even though the Ag nanoparticles were located a minimum of 200 nm from the MQWs. The magnitude of the SPE-LED output power was 1.8-fold that of the conventional LED at 350 mA, and nearly the same *I*−*V* characteristics were maintained. Excellent device performance indicated that the spin coating technique using a nano-Ag solution can be applied to fabricate LEDs that provide high-power solid-state lighting.

AUTHOR INFORMATION

Corresponding Author

*D.-S. Wuu. E-mail: dsw@dragon.nchu.edu.tw.

Author Contributions

The paper was written through contributions of all authors. All authors have given approval to the final version of the paper.

Notes

The authors declare no competing financial interest.

ACKNOWLEDGMENTS

This work was supported by the Ministry of Economic Affairs under Grant No. 102-E0605 and the Ministry of Science and Technology (Taiwan, R.O.C.) under Contract No. 102-2221-E-005-072-MY3.

REFERENCES

(1) Zhang, Y.; Gautier, S.; Cho, C.-Y.; Cicek, E.; Vashaei, Z.; McClintock, R.; Bayram, C.; Bai, Y.; Razeghi, M. Near Milliwatt Power AlGaN-based Ultraviolet Light Emitting Diodes Based on Lateral Epitaxial Overgrowth of AlN on Si(111). *Appl. Phys. Lett.* **2013**, *102*, 011106-1−011106-5.

(2) Maier-Flaig, F.; Rinck, J.; Stephan, M.; Bocksrocker, T.; Bruns, M.; Kübel, C.; Powell, A. K.; Ozin, G. A.; Lemmer, U. Multicolor Silicon Light-Emitting Diodes (SiLEDs). *Nano Lett.* **2013**, *13*, 475−480.

(3) Ying, L.; Ho, C.-L.; Wu, H. B.; Cao, Y.; Wong, W.-Y. White Polymer Light-Emitting Devices for Solid-State Lighting: Materials, Devices, and Recent Progress. *Adv. Mater.* **2014**, *26*, 2459−2473.

(4) Ra, Y.-H.; Navamathavan, R.; Yoo, H.-I.; Lee, C.-R. Single Nanowire Light-Emitting Diodes Using Uniaxial and Coaxial InGaN/GaN Multiple Quantum Wells Synthesized by Metalorganic Chemical Vapor Deposition. *Nano Lett.* **2014**, *14*, 1537−1545.

(5) Bernardini, F.; Fiorentini, V.; Vanderbilt, D. Spontaneous Polarization and Piezoelectric Constants of III-V Nitrides. *Phys. Rev. B* **1997**, *56*, R10024−R10027.

(6) Takeuchi, T.; Wetzel, C.; Yamaguchi, S.; Sakai, H.; Amano, H.; Akasaki, I.; Kaneko, Y.; Nakagawa, S.; Yamaoka, Y.; Yamada, N. Determination of Piezoelectric Fields in Strained GaInN Quantum Wells Using the Quantum-Confined Stark Effect. *Appl. Phys. Lett.* **1998**, *73*, 1691−1693.

(7) David, A.; Fujii, T.; Sharma, R.; McGroddy, K.; Nakamura, S.; DenBaars, S. P.; Hu, E. L.; Weisbuch, C.; Benisty, H. Photonic-Crystal GaN Light-Emitting Diodes with Tailored Guided Modes Distribution. *Appl. Phys. Lett.* **2006**, *88*, 061124-1−061124-3.

(8) Zhao, P.; Zhao, H. Analysis of Light Extraction Efficiency Enhancement for Thin-Film-Flip-Chip InGaN Quantum Wells Light-Emitting Diodes with GaN Micro-Domes. *Opt. Express* **2012**, *20*, A765−A776.

(9) Khurgin, J. B.; Sun, G.; Soref, R. A. Practical Limits of Absorption Enhancement near Metal Nanoparticles. *Appl. Phys. Lett.* **2009**, *94*, 071103-1−071103-3.

(10) Fukuda, M.; Aihara, T.; Yamaguchi, K.; Ling, Y. Y.; Miyaji, K.; Tohyama, M. Light Detection Enhanced by Surface Plasmon Resonance in Metal Film. *Appl. Phys. Lett.* **2010**, *96*, 153107-1−153107-3.

(11) Aihara, T.; Nakagawa, K.; Fukuhara, M.; Yu, Y. L.; Yamaguchi, K.; Fukuda, M. Optical Frequency Signal Detection through Surface Plasmon Polaritons. *Appl. Phys. Lett.* **2011**, *99*, 043111-1−043111-3.

(12) García-Vidal, J. F.; Pendry, J. B. Collective Theory for Surface Enhanced Raman Scattering. *Phys. Rev. Lett.* **1996**, *77*, 1163−1166.

(13) Lordan, F.; Rice, J. H.; Jose, B.; Forster, R. J.; Keyes, T. E. Surface Enhanced Resonance Raman and Luminescence on Plasmon Active Nanostructured Cavities. *Appl. Phys. Lett.* **2010**, *97*, 153110-1−153110-3.

(14) Damm, S.; Carville, N. C.; Manzo, M.; Gallo, K.; Lopez, S. G.; Keyes, T. E.; Forster, R. J.; Rodriguez, B. J.; Rice, J. H. Surface Enhanced Luminescence and Raman Scattering from Ferroelectrically Defined Ag Nanopatterned Arrays. *Appl. Phys. Lett.* **2013**, *103*, 083105-1−083105-4.

DOI: 10.1021/am507481n
ACS Appl. Mater. Interfaces 2015, 7, 2546−2553

(15) Neogi, A.; Lee, C.-W.; Everitt, H. O. Enhancement of Spontaneous Recombination Rate in a Quantum Well by Resonant Surface Plasmon Coupling. *Phys. Rev. B* **2002**, *66*, 153305-1−153305-4.
(16) Okamoto, K.; Niki, I.; Shvartser, A.; Narukawa, Y.; Mukai, T.; Scherer, A. Surface-Plasmon-Enhanced Light Emitters Based on InGaN Quantum Wells. *Nat. Mater.* **2004**, *3*, 601−605.
(17) Okamoto, K.; Niki, I.; Scherer, A.; Narukawa, Y.; Mukai, T.; Kawakami, Y. Surface Plasmon Enhanced Spontaneous Emission Rate of InGaN/GaN Quantum Wells Probed by Time-Resolved Photoluminescence Spectroscopy. *Appl. Phys. Lett.* **2005**, *87*, 071102-1−071102-3.
(18) Barnes, W. L. Light-Emitting Devices: Turning the Tables on Surface Plasmons. *Nat. Mater.* **2004**, *3*, 588−589.
(19) Hecker, N. E.; Höpfel, R. A.; Sawaki, N.; Maier, T.; Strasser, G. Surface Plasmon-Enhanced Photoluminescence from a Single Quantum Well. *Appl. Phys. Lett.* **1999**, *75*, 1577−1579.
(20) Yeh, D.-M.; Huang, C.-F.; Chen, C.-Y.; Lu, Y.-C.; Yang, C. C. Surface Plasmon Coupling Effect in an InGaN/GaN Single-Quantum-Well Light-Emitting Diode. *Appl. Phys. Lett.* **2007**, *91*, 171103-1−171103-3.
(21) Cho, C.-Y.; Kwon, M.-K.; Lee, S.-J.; Han, S.-H.; Kang, J.-W.; Kang, S.-E.; Lee, D.-Y.; Park, S.-J. Surface Plasmon-Enhanced Light-Emitting Diodes Using Silver Nanoparticles Embedded in p-GaN. *Nanotechnology* **2010**, *21*, 205201-1−205201-5.
(22) Kao, C. C.; Su, Y. K.; Lin, C. L.; Chen, J. J. Localized Surface Plasmon-Enhanced Nitride-Based Light-Emitting Diode With Ag Nanotriangle Array by Nanosphere Lithography. *IEEE Photonics Technol. Lett.* **2010**, *22*, 984−986.
(23) Cho, C.-Y.; Kim, K. S.; Lee, S.-J.; Kwon, M.-K.; Ko, H. D.; Kim, S.-T.; Jung, G.-Y.; Park, S.-J. Surface Plasmon-Enhanced Light-Emitting Diodes with Silver Nanoparticles and SiO_2 Nano-Disks Embedded in p-GaN. *Appl. Phys. Lett.* **2011**, *99*, 041107-1−041107-3.
(24) Hong, S.-H.; Cho, C.-Y.; Lee, S.-J.; Yim, S.-Y.; Lim, W.; Kim, S.-T.; Park, S.-J. Localized Surface Plasmon-Enhanced Nearultraviolet Emission from InGaN/GaN Light-Emitting Diodes Using Silver and Platinum Nanoparticles. *Opt. Express* **2013**, *21*, 3138−3144.
(25) Cho, C.-Y.; Zhang, Y.; Cicek, E.; Rahnema, B.; Bai, Y.; McClintock, R.; Razeghi, M. Surface Plasmon Enhanced Light Emission from AlGaN-based Ultraviolet Light-Emitting Diodes Grown on Si(111). *Appl. Phys. Lett.* **2013**, *102*, 211110-1−211110-4.
(26) Yeh, D.-M.; Huang, C.-F.; Chen, C.-Y.; Lu, Y.-C.; Yang, C. C. Localized Surface Plasmon-Induced Emission Enhancement of a Green Light-Emitting Diode. *Nanotechnology* **2008**, *19*, 345201-1−345201-4.
(27) Shen, K.-C.; Chen, C.-Y.; Chen, H.-L.; Huang, C.-F.; Kiang, Y.-W.; Yang, C. C.; Yang, Y.-J. Enhanced and Partially Polarized Output of a Light-Emitting Diode with Its InGaN/GaN Quantum Well Coupled with Surface Plasmons on a Metal Grating. *Appl. Phys. Lett.* **2008**, *93*, 231111-1−231111-3.
(28) Kown, M.-K.; Kim, J.-Y.; Kim, B.-H.; Park, I.-K.; Cho, C.-Y.; Byeon, C. C.; Park, S.-J. Surface-Plasmon-Enhanced Light-Emitting Diodes. *Adv. Mater.* **2008**, *20*, 1253−1257.
(29) Ryu, H.-Y.; Choi, I.-G.; Choi, H.-S.; Shim, J.-I. Investigation of Light Extraction Efficiency in AlGaN Deep-Ultraviolet Light-Emitting Diodes. *Appl. Phys. Express* **2013**, *6*, 062101-1−062101-4.
(30) Shakya, J.; Knabe, K.; Kim, K. H.; Li, J.; Lin, J. Y.; Jiang, H. X. Polarization of III-nitride Blue and Ultraviolet Light-Emitting Diodes. *Appl. Phys. Lett.* **2005**, *86*, 091107-1−091107-3.
(31) Sung, J.-H.; Kim, B.-S; Choi, C.-H.; Lee, M.-W.; Lee, S.-G.; Park, S.-G.; Lee, E.-H.; O, B.-H. Enhanced Luminescence of GaN-based Light-Emitting Diode with a Localized Surface Plasmon Resonance. *Microelectron. Eng.* **2009**, *86*, 1120−1123.
(32) Sung, J.-H.; Yang, J. S.; Kim, B.-S.; Choi, C.-H.; Lee, M.-W.; Lee, S.-G.; Park, S.-G.; Lee, E.-H.; O, B.-H. Enhancement of Electroluminescence in GaN-based Light-Emitting Diodes by Metallic Nanoparticles. *Appl. Phys. Lett.* **2010**, *96*, 261105-1−261105-3.
(33) Gao, N.; Huang, K.; Li, J. C.; Yang, X.; Kang, J. Y. Surface-Plasmon-Enhanced Deep-UV Light Emitting Diodes Based on AlGaN Multi-Quantum Wells. *Sci. Rep.* **2012**, *2*, 816.
(34) Kumar, M.; Zhao, H.; Persson, C. Study of Band-structure, Optical Properties and Native Defects in $A^IB^{III}O_2$ (A^I = Cu or Ag, B^{III} = Al, Ga or In) Delafossites. *Semicond. Sci. Technol.* **2013**, *28*, 065003.
(35) Fukumura, T.; Toyosaki, H.; Yamada, Y. Magnetic Oxide Semiconductors. *Semicond. Sci. Technol.* **2005**, *20*, S103−S111.
(36) Houng, B. Tin Doped Indium Oxide Transparent Conducting Thin Films Containing Silver Nanoparticles by Sol-Gel Technique. *Appl. Phys. Lett.* **2005**, *87*, 251922-1−1251922-3.

DOI: 10.1021/am507481n
ACS Appl. Mater. Interfaces 2015, 7, 2546−2553